RESEARCH ARTICLE | MARCH 27 2025

Atomic layer deposition of $Al_xTi_{1-x}N$ via co-evaporation of metal precursors

Special Collection: Atomic Layer Deposition (ALD)

Pamburayi Mpofu ; Pentti Niiranen ; Oscar Alm ; Jonas Lauridsen ; Tommy Larsson ; Henrik Pedersen

J. Vac. Sci. Technol. A 43, 032405 (2025)
https://doi.org/10.1116/6.0004420

JVST A
Journal of Vacuum Science & Technology A
ARTICLE
pubs.aip.org/avs/jva

Atomic layer deposition of $Al_xTi_{1-x}N$ via co-evaporation of metal precursors

Cite as: J. Vac. Sci. Technol. A **43**, 032405 (2025); doi: 10.1116/6.0004420
Submitted: 23 January 2025 · Accepted: 7 March 2025 ·
Published Online: 27 March 2025

View Online Export Citation CrossMark

Pamburayi Mpofu,[1,a)] Pentti Niiranen,[1] Oscar Alm,[2] Jonas Lauridsen,[2] Tommy Larsson,[2] and Henrik Pedersen[1,a)]

AFFILIATIONS

[1] Department of Physics, Chemistry and Biology, Linköping University, Linköping SE-581 83, Sweden
[2] Seco Tools AB, Fagersta SE-737 82, Sweden

Note: This paper is part of the 2025 Special Topic Collection on Atomic Layer Deposition (ALD).

[a)] **Authors to whom correspondence should be addressed:** pamburayi.mpofu@liu.se and henrik.pedersen@liu.se

ABSTRACT

Different approaches are used in tailoring properties of thin films to meet the requirements of specific applications. This study comprises work done on atomic layer deposition of $Al_xTi_{1-x}N$ employing the co-evaporation approach using tris-dimethylamido aluminum [$Al(NMe_2)_3$], tetrakis(dimethylamido)titanium (IV) [$Ti(NMe_2)_4$], and ammonia (NH_3) plasma. High Al-content, low impurity (O and C, both <5 at. %) films with uniform grain size distribution and dense morphology were deposited. The as-deposited films were x-ray amorphous, but mixed crystallographic phases were observed when the films were annealed at 700 °C. The deposited aluminum-rich $Al_xTi_{1-x}N$ films show an alternative way for ternary material depositions.

I. INTRODUCTION

Protective coating materials are commonly grown using physical or chemical vapor deposition (PVD or CVD) techniques on cutting tools. This improves the service life of the tools during high temperatures, friction, wear, corrosion, and oxidation leading to mechanical and thermal fatigue, during applications such as turning, milling, and drilling.[1] Such coatings have been used in the form of nitrides, oxynitrides, carbides, carbonitrides, borides, boronitrides, and oxides, where a lot of comparisons[2] between PVD and CVD have been made. It can be noted that many of the nitride, oxide, and carbide protective hard coatings produced for the engineering and manufacturing industry are also highly relevant for the microelectronics field, e.g., as dielectrics, diffusion barriers,[3] and gate oxides.[4] AlN is one example of such a material used in microelectronic and optoelectronic applications because of its wide bandgap (6.2 eV),[5] high dielectric constant (~9),[6] high electrical resistivity (~10^{11}–10^{13} Ω cm),[7] good thermal conductivity (2.85 W/K cm),[8] and piezoelectric properties.[9]

AlN also has good miscibility with other nitrides, making it interesting to many ternary materials with, e.g., Ga,[10] In,[11] Ti,[12] or Hf,[13] thereby increasing the range of its possible applications. One such ternary material is metastable $Al_xTi_{1-x}N$ where the cubic rock salt structure of TiN is preserved while varying Al content. $Al_xTi_{1-x}N$ primarily finds use as a hard material in protective coatings, often on cemented carbide tool inserts due to its excellent resistance against corrosion and oxidation and high hardness.[14–16] These properties can be tuned with the chemical composition.

The synthesis of nitrides in the form of metastable high Al-content $Al_xTi_{1-x}N$ by CVD, where the cubic structure of TiN is preserved while adding AlN, i.e., increasing x, up to at least 0.9,[17] has gained increasing interest in recent years.[18,19] The presence of AlN increases oxidation resistance of the formed $Al_xTi_{1-x}N$ film by converting to an Al_2O_3 layer as the coating heats up resulting in increased oxidation resistance.[20] Different techniques such as PVD that include reactive sputtering,[21] ion plating,[22] cathodic arc evaporation,[23] and CVD[24–26] have been employed in the deposition of $Al_xTi_{1-x}N$ as a wear resistant coating. CVD of $Al_xTi_{1-x}N$ is less understood; hence, atomic layer deposition (ALD)—a modification of CVD—can be used as a tool or model system to study and understand the surface chemistry and reaction mechanisms in CVD. ALD combines precise film thickness control, high conformality, and high uniformity in film quality and composition over large areas. In ALD, gaseous precursors are alternately supplied onto a solid substrate. This offers surface self-limiting layer-by-layer growth, which in turn enables the study of surface chemistry and reaction mechanisms in CVD of $Al_xTi_{1-x}N$ using *in situ* techniques in ALD.

The most common ALD approach for synthesizing multicomponent materials involves combining the ALD processes for the binary materials into a supercycle, enabling precise control over the material composition by adjusting the ratio of the binary materials.[27,28] This approach depends on the diffusion of the two binary materials to form a homogeneous ternary phase, rather than a multilayer of the binary materials. Reports on ALD of $Al_xTi_{1-x}N$ are scarce. $Al_xTi_{1-x}N$ has only three entries in the Atomic Limits database,[29] all for semiconductor-related applications, and all using supercycles. Xiang *et al.*[30] successfully developed thermal processes with trimethyl aluminum (TMA), $TiCl_4$, and NH_3 as precursors. The presence of NH_3 in the reaction led to the formation of AlTiN(C) films, while its absence resulted in AlTiC films, suitable for metal gates and low power FinFET applications. The deposition modes in that study included multiple precursor pulses and purges, which are characteristic of the supercycle method. Furthermore, supercycles consisting of two groups of subcycles dedicated to TiN and AlN, using TMA, tetrakis(dimethylamido)titanium(IV) (TDMAT), and N_2 plasma were applied by Yun *et al.*,[31] resulting in stoichiometric AlTiN, suitable for applications where both electrical performance and durability against corrosion are critical. In the third study, Juppo *et al.*[32] deposited (Al)TiN using TMA, $TiCl_4$, and NH_3, focusing on the role of TMA as a reducing agent. The highest growth rates were achieved using a supercycle pulsing scheme, where NH_3 is pulsed after both $TiCl_4$ and TMA, forming films with good barrier properties usable in preventing interdiffusion between copper and silicon.

Here, we present an alternative ALD approach to deposit metastable high Al-content $Al_xTi_{1-x}N$ based on tris-dimethylamido aluminum (TDMAA) and TDMAT precursors that were co-evaporated into the reaction chamber in a single dose. This precursor choice was first motivated by the fact that more common $Al_xTi_{1-x}N$ deposition processes rely on chlorine-based precursors such as $TiCl_4$ and $AlCl_3$, which not only require high temperatures but can also lead to Cl incorporation in the films.[33,34] Second, our a previous publication from our research group[35] proved that alloying group 13-nitrides (by co-subliming gallium and indium precursors with identical ligands) leading to ternary phases enabled tuning properties of the resulting $In_{1-x}Ga_xN$ films. Third, previous studies[36,37] suggest that organoaluminum compounds with dimethylamino and methyl substitutions, such as TDMAA, are stable in TDMAT, allowing TDMAA and TDMAT to be mixed. Finally, mass spectrometry investigations[24] have confirmed that TDMAA and TDMAT do not react with each other in the vapor phase. To the best of our knowledge, no ALD study of $Al_xTi_{1-x}N$ grown with this precursor combination and process approach has been reported to date.

II. EXPERIMENTAL DETAILS

A. Film deposition

A hot-wall Picosun R-200 Advanced ALD reactor, equipped with a Litmas remote inductively coupled plasma (ICP) source, was used for the depositions. The reactor operated at 4 mbar with a continuous flow of 400 SCCM high purity N_2 (99.999%, further dried using a getter filter) into the chamber, which was also used as the purge gas. TDMAA and TDMAT from Sigma-Aldrich (99.999%) with sublimation temperatures of 120 and 60 °C, respectively, were used for developing the binaries AlN and TiN.[38] To vary the stoichiometry in the films, the sublimation temperature was varied between 90 and 120 °C for the TDMAA + TDMAT mixture. The ALD of $Al_xTi_{1-x}N$ was then carried out using the same optimized parameters as for the binary nitrides, with NH_3 plasma serving as the nitrogen source. The ALD process used a plasma discharge in a mixture of 75 SCCM NH_3 and 100 SCCM Ar (99.999%, further purified by a getter filter). The ICP source was located approximately 75 cm above the substrate and ignited the plasma with a 2800 W plasma power. Prior to deposition, approximately $2 \times 2\ cm^2$ Si (100) substrates were cleaned with acetone and isopropanol for 10 min each to remove surface contaminants before blow-drying them with N_2 gas. To avoid unwanted effects, the reactor was conditioned by long passivation runs of either N_2/NH_3 plasma or thermal treatment in N_2 flow for at least 24 h while maintaining it at 4 mbar operating pressure and 200 °C on both substrate and wall temperature.

Prior to the deposition of $Al_xTi_{1-x}N$ films, the growth characteristics of both AlN and TiN were investigated to ensure self-limiting film growth. Our recent ALD surface chemistry study[38] has shown that both TDMAA and TDMAT do sublime with a sufficient vapor pressure at 120 and 60 °C for AlN and TiN depositions, respectively. The ALD of $Al_xTi_{1-x}N$ was then carried out using these optimized parameters at sublimation temperatures between 90 and 120 °C for the TDMAA + TDMAT mixture and the chemical composition was monitored. A low deposition temperature of 200 °C, below the decomposition point for both TDMAA and TDMAT, and where both precursors show self-limiting growth, was then selected.

B. Film characterization

Crystallinity was measured in both $\theta - 2\theta$ x-ray diffraction (XRD) and grazing incidence XRD (GIXRD) geometries using a PANalytical EMPYREAN MRD diffractometer with a Cu x-ray tube, wavelength 1.54 Å operating at 45 kV and 40 mA and using the mirror and parallel plate collimator, on incident and diffracted beam optics, respectively. X-ray photoelectron spectroscopy (XPS) was used for surface analyses comprising elemental compositions and chemical bonding. The spectrometer was a Kratos AXIS Ultra DLD, equipped with an Ar sputtering source and employing monochromatic Al Kα x-ray radiation with 150 W power (anode current = 10 mA and anode voltage = 15 kV). To remove the surface oxide and other surface contaminants, which is a result of air exposure and to do a depth profile, sputter etching with a beam energy of 0.5 keV was used. Survey scans for qualitative analysis were carried out in the range 1200 to −5 eV, with a 1 eV step size and a dwell time of 300 ms. The recorded photoelectron spectra were analyzed, using the CASAXPS software package. By quantitative analysis in CASAXPS, the signals originating the thin films could be de-convoluted and the chemical composition could be quantified. Gaussian–Lorentz functions and Shirley background were used to fit the experimental XPS data. Surface morphologies were obtained by a Zeiss Gemini SEM 560 scanning electron microscope (SEM) with an acceleration voltage set to 3 kV, a working distance of ~3 mm, and producing images with the in-lens detector.

III. RESULTS AND DISCUSSION

Core-level XPS spectra of the chemical states and bonding of the Al, Ti, N, and O atoms in the films were recorded and studied. Figure 1 shows XPS analysis results of $Al_xTi_{1-x}N$ films deposited from four different mixing molar ratios (2:1; 3:1; 4:1; and 10:1 and ascribed as samples 1–4, respectively). In each of the core-level elemental peaks, peak positions do not change significantly with changes in precursor molar ratios indicating that the different elements are in the same bonding state or chemical environment. The Ti 2p and N 1s peaks were slightly asymmetric, indicating the presence of different bonding features or contributions in the films.

For a more accurate analysis of the chemical bonding status, such as metal nitrides and possible metal oxide in the films, all narrow scans were deconvoluted as illustrated by the selected sample 4 shown in Fig. 2. A key consideration involves understanding the nature of the oxygen impurities in the films and their potential chemical interactions with Al, Ti, and N. High-resolution XPS analysis of the Al 2p, Ti 2p, and N 1s peaks provided insights into these bonding characteristics. Al 2p regions in the spectra of all films showed symmetrical peaks indicating a clean and almost full Al–N character assigned at 74.1–74.3 eV.[39–41] As shown in Fig. 2(a) mainly Al–N bonds and negligible Al–N–O (which is otherwise expected at around 75.4 eV) bonds were observed.[42] On the contrary,

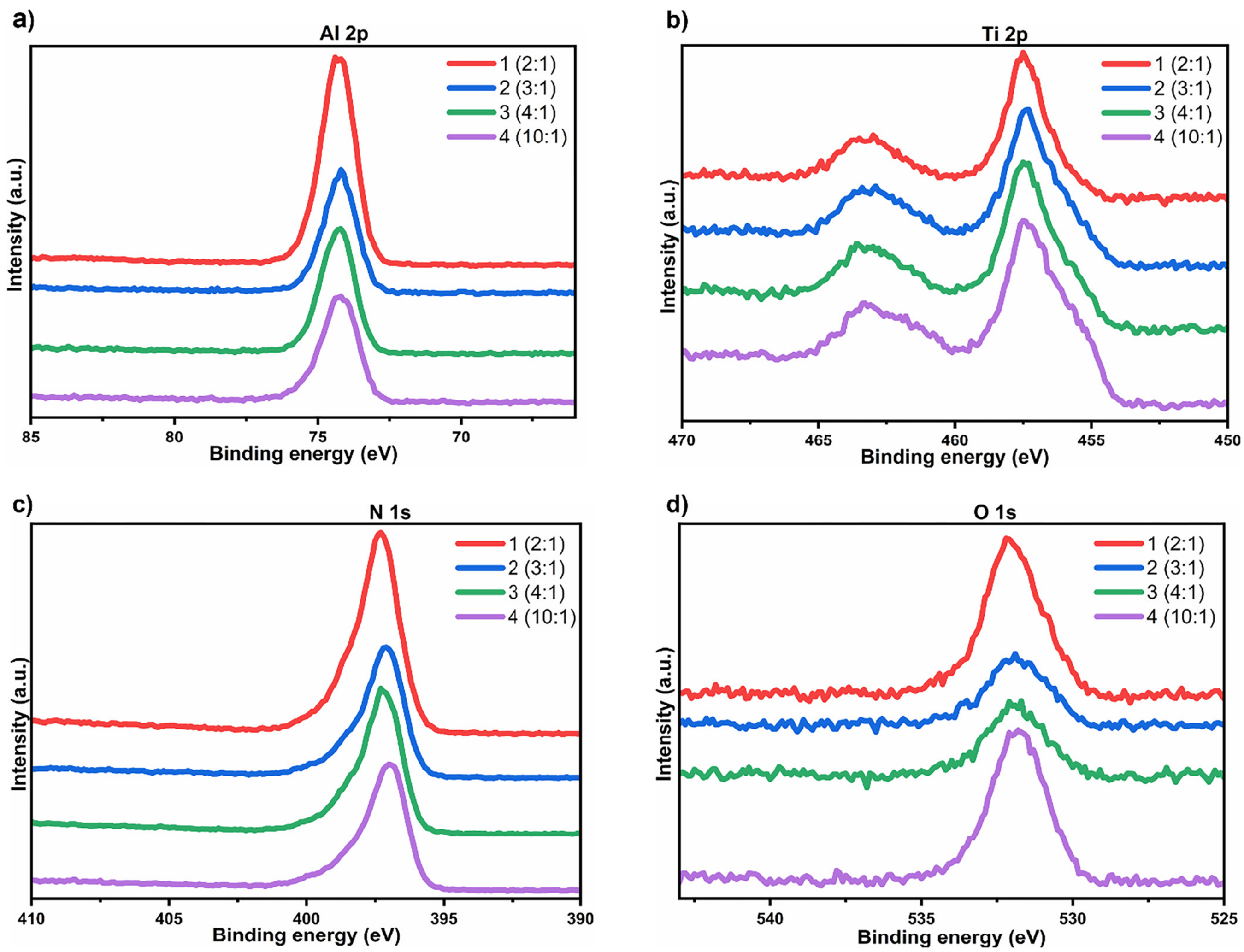

FIG. 1. Narrow range core-level photoelectron spectra acquired from the $Al_xTi_{1-x}N$ films that were deposited from different molar ratios in four different samples (a) Al 2p, (b) Ti 2p, (c) N 1s, and (d) O 1s. Carbon contribution is almost below the detection limit in the majority of the samples and, therefore, the C 1s spectrum was omitted.

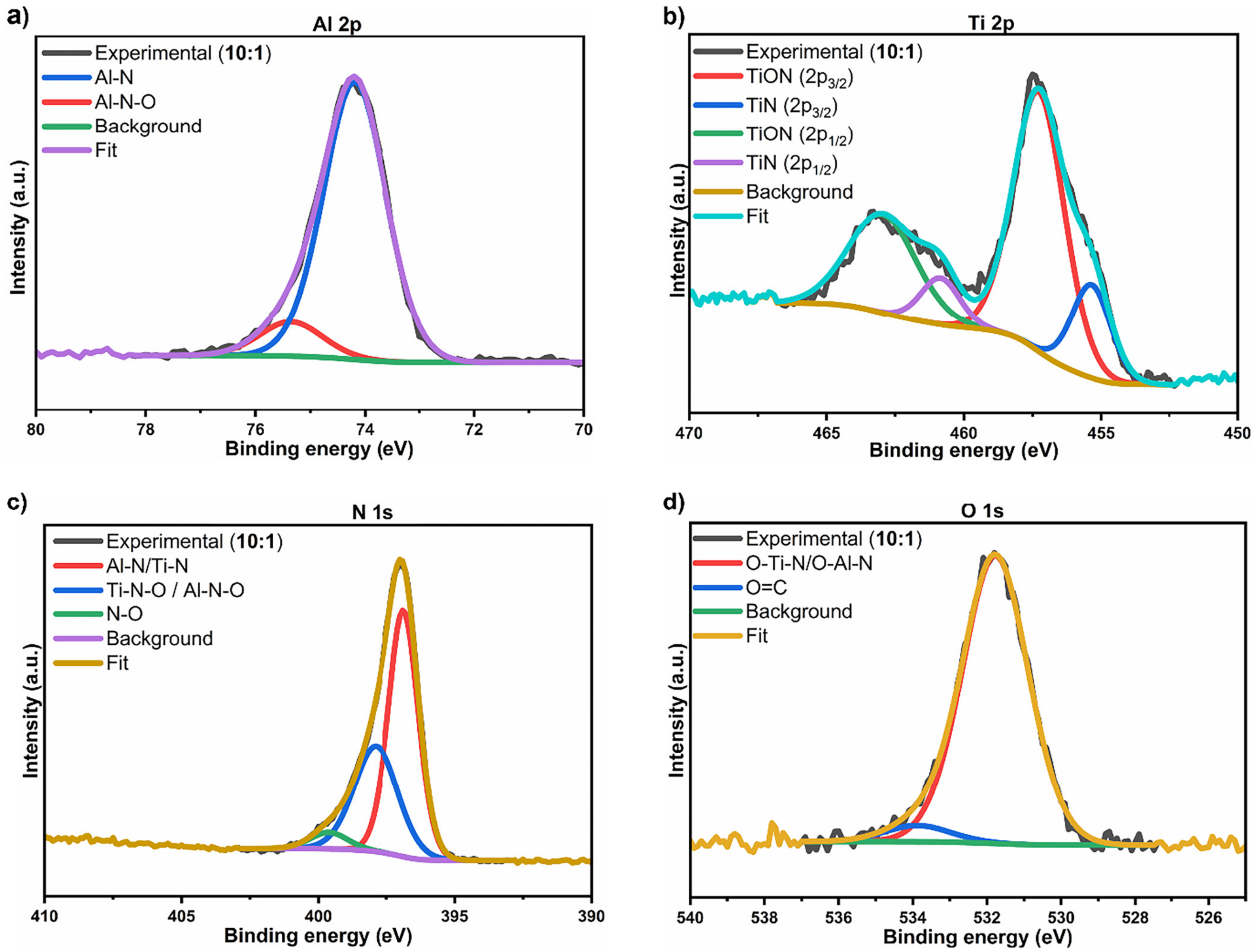

FIG. 2. Deconvoluted high-resolution XPS spectra of an $Al_xTi_{1-x}N$ film sample that was deposited from 10:1 molar ratio providing insights into the bonding characteristics (a) Al 2p, (b) Ti 2p, (c) N 1s, and (d) O 1s.

deconvolution of the Ti 2p spectrum, shown in Fig. 2(b), gives rise to four peaks or two doublets, due to spin–orbit splitting, that were identified as corresponding to Ti–N ($2p_{3/2} = 455.4$ eV and $2p_{1/2} = 460.9$ eV) and Ti–O–N ($2p_{3/2} = 457.3$–457.4 eV and $2p_{1/2} = 462.9$–463.4 eV).[43–46] The Ti–N concentration, i.e., peak area is lower than the Ti-O-N concentration on the film surface revealing that Ti is exhibiting more oxide character than the nitride contribution. This is understandable considering TDMAT's high affinity for moisture and oxygen, as will be discussed later. Three subpeaks were used in fitting the N 1s peak, observed from the pure N–Al/N–Ti at a binding energy of 396.9 eV while other subpeaks observed at higher binding energies were assigned to the three component titanium oxynitride system (N–Ti–O) and the ignorable oxynitride component of Al (N–Al–O) at 397.9 and 399.6, respectively.[41,47] The O 1s peak at 531.8 eV is quite symmetric and corresponds to O–Ti–N bonding[43] and possibly O–Al–N with an excludable minor contribution of an XPS peak possibly corresponding to oxygen bonded to carbon.

Elemental quantification, i.e., chemical compositional analysis of the deposited films from different precursor mixing ratios was recorded. Figure 3 shows the XPS depth profiles of films deposited at 200 °C, confirming that $Al_xTi_{1-x}N$ was deposited with relatively uniform elemental distribution throughout the film. The two plots [Figs. 3(a) and 3(b)] show two samples prepared from 3:1 and 4:1 TDMAA:TDMAT molar ratios, giving almost similar chemical compositions, illustrating that mixing ratios might actually not play a significant role in determining film composition. Another important observation to note is the considerably low impurity (C and O, both less than 5 at. %) content in the films, an indication of a well-functioning nitride deposition process. In microelectronics

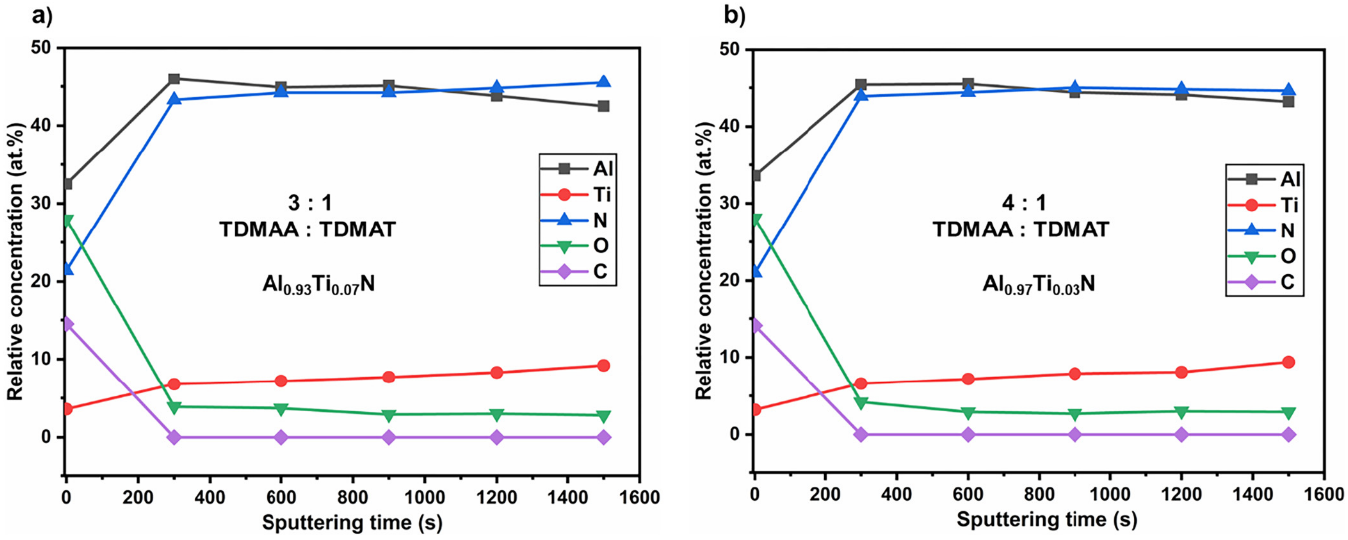

FIG. 3. XPS depth profiles of $Al_xTi_{1-x}N$, showing similar high Al-content films with almost 1:1 Al:N ratio and C impurities below detection limit within the bulk of the films. A 3:1 mole ratio (TDMAA:TDMAT) was used in (a) while a 4:1 mole ratio was used in (b).

applications, increased carbon content can create defects or alter the microstructure of the films, which may provide pathways for diffusion, thereby reducing their barrier effectiveness. In some cases, carbon can enhance the oxidation resistance of $Al_xTi_{1-x}N$ coatings. However, if the carbon content is too high, it may lead to the formation of carbon oxides, which can degrade the protective properties of the coating by formation of softer phases or reduce the density of the coating.[48]

TDMAT is highly reactive with water and oxygen exposure, which can lead to unwanted reactions and contamination during film growth, complicating the deposition process. This could possibly explain the O contamination (even though low, below 5 at. %) in almost all the films, e.g., as shown in Fig. 3. In contrast, TDMAA is only slightly air sensitive and more stable due to its dimer structure, which protects the aluminum atom from rapid reactions with moisture and oxygen.[49] This stability allows TDMAA to maintain its integrity longer during deposition. The higher thermal stability of TDMAA has been shown in different studies[50–52] by film deposition at higher temperatures using TDMAA compared to TDMAT, indicating that TDMAA can endure higher thermal conditions without decomposing, facilitating more controlled film growth.

When TDMAA and TDMAT are exposed to NH_3, they undergo a complete transamination reaction,[38] transferring amino groups and forming new compounds with less carbon while releasing dimethylamine. Transaminated compounds decompose at significantly lower temperatures compared to their nontransaminated counterparts. As a result, the overall activation energy required for the decomposition of these dimethyl amido precursors is reduced, allowing for film deposition to occur at lower temperatures which can be advantageous for deposition on temperature sensitive substrates. This can enhance the quality of the films produced and improve the incorporation of desired elements into the film structure while minimizing unwanted carbon content and other impurities.[53–57]

Figure 4 shows the XPS depth profiles, illustrating the effects of molar ratio changes from 2:1 to 10:1 TDMAA:TDMAT on $Al_xTi_{1-x}N$ film composition. The chemical composition of the grown films, as shown by XPS, still shows Al-rich films but with slightly reduced Al contribution and increased Ti content. This change in film composition was the opposite of the change in precursor mixture.

XPS depth profile analysis (Figs. 3 and 4) reveals that the surface composition before sputtering predominantly comprises oxides, i.e., metal oxide and oxidized metal nitride, while the bulk of the films have low oxygen content and C content almost below the detection limit of XPS. This scenario is consistent with surface oxidation of $Al_xTi_{1-x}N$ when exposed to air, resulting in a protective oxide layer on the film surface.[58]

Figure 5 shows XPS depth profiles for $Al_xTi_{1-x}N$ samples that were grown from the same precursor mixture without refilling the bubbler. The Ti component of the films decreases gradually with continued deposition, which is explained by the differences in reactivity between TDMAA and TDMAT with NH_3, which leads to the depletion of the Ti precursor.

The mixture of TDMAA and TDMAT is generally a dispersion that becomes liquid in excess TDMAT. TDMAA is a solid at room temperature and has a lower vapor pressure than the liquid TDMAT, resulting in preferential TDMAT evaporation, meaning if there is a need to increase the Ti content in the films, excess TDMAT is required, otherwise eventually deposited films will just be AlN. Figure 5 illustrates how the differences in precursor volatilities affect film composition.

From the XPS results, it appears that the films were very rich in Al regardless of the mixing ratio of TDMAT to TDMAA. This can be explained by several reasons:

(i) *Nucleation delay differences*—both AlN ALD[38] and TiN ALD[59] have shown that nucleation is easy (no nucleation

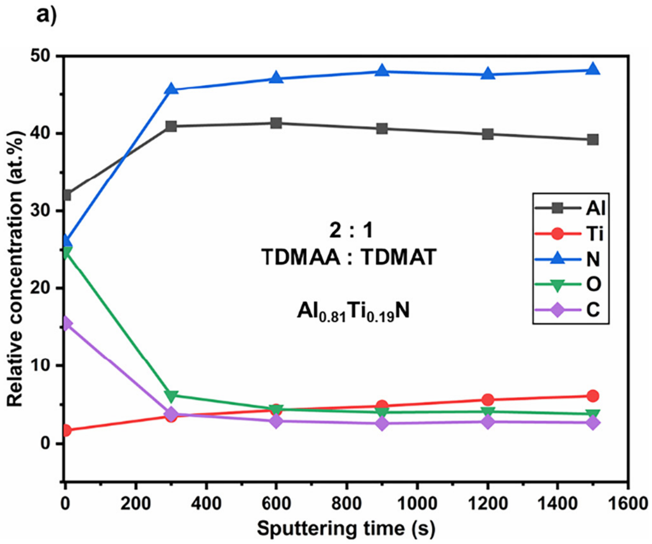

FIG. 4. XPS depth profiles of $Al_xTi_{1-x}N$, showing N-rich thin films with low levels of C and O contamination. A 2:1 mole ratio (TDMAA:TDMAT) mixture was used in (a) while a 10:1 mole ratio was used in (b).

delays), as shown by both ALD processes exhibiting substrate-enhanced growth, i.e., growth per cycle (GPC) that is high at the very start of the deposition. However, plotting the number of cycles against film thickness for the two processes gives intercepts at around −111 cycles for AlN and approximately −5 cycles for TiN, which therefore points to the fact that AlN nucleates faster than TiN, hence less Ti may be incorporated in the film.

(ii) *Possible substrate effects*—AlN and TiN possibly nucleate differently on different substrates. In trying to address this, in addition to Si, we tried deposition on different substrates: Al_2O_3, SiC, and TiN-coated Si. The Ti at. % in all three samples was similar (8.8%, 8.6%, and 8.5%, respectively), showing that AlN always nucleates faster and more efficiently than TiN regardless of the substrates, at least, for the investigated substrates.

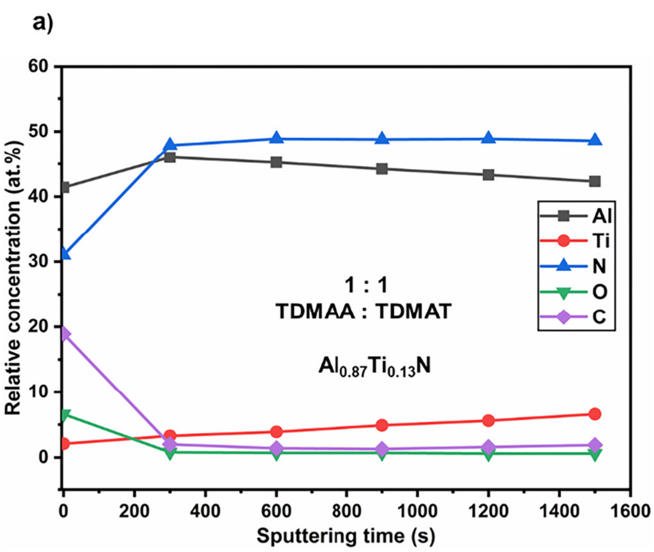

FIG. 5. XPS depth profiles of $Al_xTi_{1-x}N$ thin films grown from the same bubbler, using the same co-evaporated 1:1 mole ratio TDMAA:TDMAT mixture with results from the first run shown in (a) while the second run is shown in (b), without refilling the bubbler.

(iii) *Kinetic differences*—a reaction kinetics favoring the incorporation of Al will lead to a higher Al content in the $Al_xTi_{1-x}N$ films. The reaction between $Ti(NMe_2)_4$ and NH_3 has been reported with an activation energy of 33.5 kJ mol^{-1}.[60,61] In our recent work[38] on AlN ALD from $Al(NMe_2)_3$ and NH_3, we reported a lower activation barrier of 27 $kJmol^{-1}$, meaning that TDMAA reacts more readily. This suggests that Al is more easily incorporated into the films. In this present study, we investigated how the reaction rate (or Ti incorporation) changes with temperature for depositions with a 1:1 precursor molar ratio at 200, 250, and 300 °C. The Ti atomic composition was found to be 3.9%, 5.8%, and 7.2%, respectively. The differences are not that remarkable but there is a trend that might point toward kinetics preventing Ti from being incorporated.

(iv) *Steric effects*—the three dimethylamido ligands of TDMAA suggest a planar coordination around a sp^2-hybridized Al atom. The four ligands of TDMAT suggest a tetrahedral coordination around a sp^3-hybridized Ti atom. The sp^2-hybridized Al atom with a lone p-orbital should be more susceptible to a nucleophilic attack from a surface amine group with a free electron pair on the nitrogen atom. This suggests that Al is more easily incorporated into the films.

(v) *Thermodynamics*—Ti incorporation is generally more favorable than Al incorporation due to the somewhat higher stability of Ti compounds, lower Gibbs free energy of formation (at standard conditions, ΔG for TiN ≈ −339 kJ/mol and ΔG for AlN ≈ −318 kJ/mol),[62] and favorable reaction energies. The actual incorporation rates will also depend on kinetic factors and processing conditions. Even if Ti incorporation is thermodynamically favored, the kinetics of the reaction may be slower compared to Al, which could lead to differences in the final material properties.

Finally, it is important to note that, from our results, the relationship between mixing ratios and chemical composition seems contradictory or looks like there is no direct relationship at all between these two variables. This speaks to the difficulty in stoichiometry control that one faces when using this approach, hence the

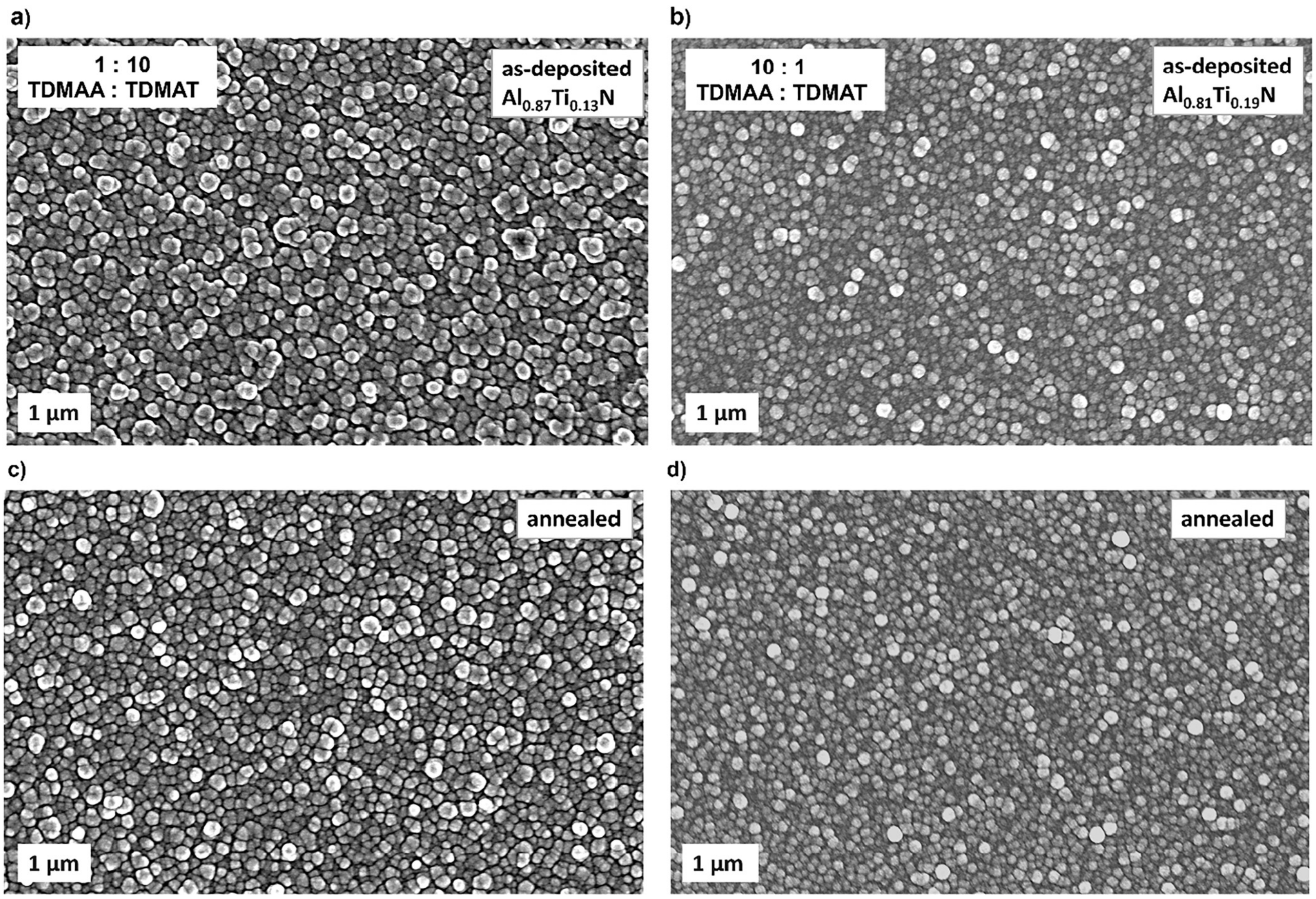

FIG. 6. SEM images of $Al_xTi_{1-x}N$ thin films grown from a 1:10 mole ratio (TDMAA:TDMAT) mixture before and after annealing shown in (a) and (c) while films from a 10:1 mole ratio before and after annealing are shown in (b) and (d), respectively.

above considerations must be taken into account for each given material system when one is using the co-evaporation method.

Figure 6 shows the SEM images of the as-deposited $Al_{0.87}Ti_{0.13}N$ and $Al_{0.81}Ti_{0.19}N$ [Figs. 6(a) and 6(b)] thin films deposited from a 1:10 and 10:1 (TDMAA:TDMAT) molar ratio, respectively, in comparison with their annealed counterparts [Figs. 6(c) and 6(d)]. The two sets of samples have a uniform surface morphology. The top view electron micrographs show that the high Al-content $Al_xTi_{1-x}N$ thin films grew with uniform grain size distribution and dense morphology. The films exhibit big and distinct grains -that were measurable to approximately between 0.10 and 0.15 μm, with uniform distribution of surface features. Additionally, no distinct pinholes or macroparticles are observed in the images. The morphology of the films did not change with annealing [Figs. 6(c) and 6(d)], indicating that the films have good thermal stability (withstanding elevated temperatures with no morphological changes). Additionally, no changes in morphology could suggest limited atomic diffusion within the film (due to a high activation energy barrier for diffusion or a lack of sufficient thermal energy to facilitate atomic movement, which can hinder processes like grain growth or surface rearrangement). It can also mean the stability of existing phases (no driving force for transformation or growth, leading to a consistent morphology).[63] Cross-sectional SEM measurements gave sample thicknesses between approximately 50–350 nm, which are remarkably thick films by typical ALD standards. This is illustrated by the GPC versus mixing ratio shown in Fig. 7(a) while Fig. 7(b) shows how the Ti content in the films is affected by the mixing ratio. The GPC increases with an increase in the molar ratio, i.e., a decrease in the Ti precursor ratio, which also renders an increase in the Ti content in the films. Based on the individual GPCs of TiN and AlN, the film growth results in Fig. 7 would seem somewhat counter-intuitive. A previous study[31] has shown that the growth characteristics of TiN saturate at 0.5 Å/cycle, which is lower than that of AlN at approximately 1 Å/cycle, while the GPC for AlTiN GPC was then found to be 5 Å/cycle. This was also illustrated in another AlTiN ALD study,[64] which gave a GPC of 3.5 Å/cycle, even though the growth rates for TiN and AlN reached saturation levels of 2.4 and 1.5 Å/cycle, respectively. It is common to observe a similar discrepancy and fluctuation between the measured and calculated or expected growth rates in various multicomponent films prepared by ALD.[65] This variation possibly arises from the differences in the quantity of chemisorbed precursors on heterogeneous versus homogeneous surfaces.[31] For example, it is not far-fetched to think that a smaller amount of TDMAT chemisorbs on an AlN surface compared to the more uniform TiN surface and vice versa. Therefore, it can be speculated that the titanium content in the films may shift the growth dynamics to favor an effective growth rate due to the enhanced availability of the reactive species during the co-evaporation approach.

Figure 8 displays the GIXRD patterns of the as-deposited $Al_xTi_{1-x}N$ thin films with different compositions as deposited and after annealing at 700 °C in N_2 for 2 h. The GIXRD pattern of sample 1 ($Al_{0.81}Ti_{0.19}N$) after annealing shows peaks corresponding to a hexagonal AlN. An additional weak peak at 45° could be ascribed to (200) of cubic $Al_xTi_{1-x}N$, suggesting the possibility of mixed phases in the annealed film. The other films still appear x-ray amorphous after annealing.

The x-ray amorphous nature of the films could suggest an almost full incorporation of AlN. When aluminum is incorporated into the TiN lattice to form $Al_xTi_{1-x}N$, the smaller ionic radii (0.54 Å for Al^{3+} compared to 0.67 Å for Ti^{3+})[66,67] allow it to substitute for titanium atoms in the lattice. This substitution can disrupt the regular arrangement of atoms, leading to increased disorder within the material. Computational methods by Forslund and Ruban[68] on how Ti inclusions affect the cubic structure and the overall properties of $Al_xTi_{1-x}N$ alloys have been used to understand the thermodynamic driving forces influencing coating formation during the CVD process.

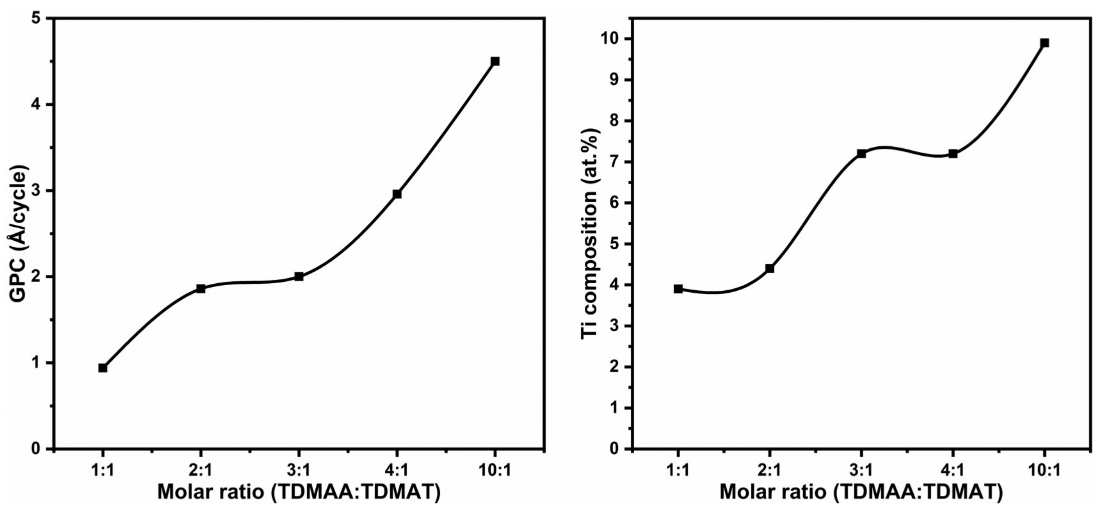

FIG. 7. Relationship between (a) GPC and (b) Ti content, with changes in precursor mixing molar ratios.

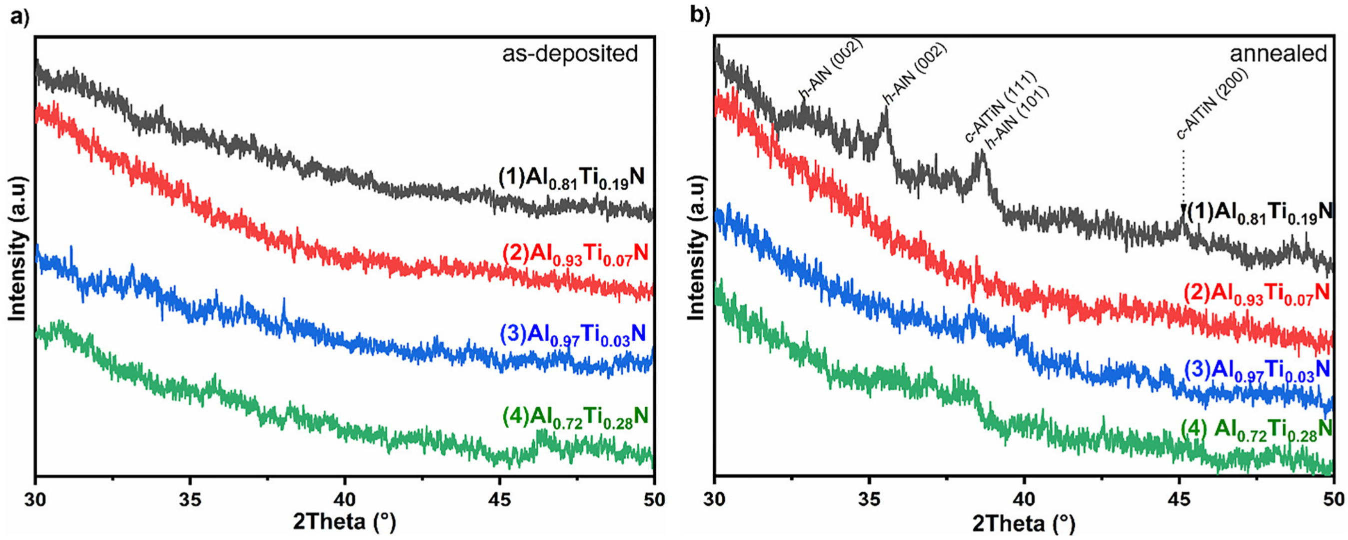

FIG. 8. GIXRD patterns of as deposited $Al_xTi_{1-x}N$ films with different elemental compositions before annealing (a) and GIXRD results from high temperature annealing of $AlxTi_{1-x}N$ samples up to 700 °C (b). Sample 1, (black line), showed signs of h-AlN and possibly c-AlTiN with weak, broad peaks.

Their calculations were compared with experimental observations, particularly regarding the preferential growth of certain facets and the segregation of Ti atoms to the surface during the growth of Al-rich films. They revealed that the surface energies of random $Al_xTi_{1-x}N$ alloys exhibit minimal dependence on composition, with a significant increase in Ti segregation tendency occurring near pure AlN. The greater the concentration of Al, the more pronounced the segregation of Ti to the surface becomes. In our case, as a result, the presence of high aluminum content hinders the formation of a well-defined crystalline structure, promoting an amorphous phase instead.[32] This amorphous nature leads to a loss of long-range crystalline order of TiN.[31] Notably, an amorphous structure is often considered advantageous for certain applications, e.g., corrosion-resistant coatings due to the absence of defective grain boundaries.[69] Even though this is a shortcoming in hard coating applications, the behavior is significant in other applications where such specific material properties are desired, for example, diffusion barriers in microelectronics.

IV. CONCLUSIONS

In summary, we developed a new ALD process to deposit high Al-content $Al_xTi_{1-x}N$ by co-evaporating dimethylamidometal complexes, TDMAA and TDMAT, and adding NH_3 plasma as the nitrogen source—offering an alternative to the more common supercycle approach. We successfully deposited low impurity (<5 at. %) $Al_xTi_{1-x}N$ thin films at temperatures as low as 200 °C. The cubic $Al_xTi_{1-x}N$ phase could not be explicitly exhibited from our results, and more work needs to be done to improve the cubic phase and/or minimize the hexagonal phases if these films are to be useable in hard coating applications. Our results suggest that TDMAA and TDMAT are promising precursors for low-temperature/low-pressure co-evaporation ALD of $Al_xTi_{1-x}N$ and more ternaries can be deposited using the same method. These findings offer a promising alternative to the more common supercycle approach and overall, important insights into multicomponent ALD processes.

ACKNOWLEDGMENTS

Seco Tools and the Swedish Foundation for Strategic Research through the project "Time-resolved low temperature CVD for III-nitrides" (SSF-RMA 15-0018) are gratefully acknowledged for financial support. H.P. acknowledges financial support from the Swedish Government Strategic Research Area in Materials Science on Advanced Functional Materials at Linköping University (Faculty Grant SFO-Mat-LiU No. 2009-00971).

AUTHOR DECLARATIONS

Conflict of Interest

The authors have no conflicts to disclose.

Author Contributions

Pamburayi Mpofu: Conceptualization (lead); Data curation (lead); Formal analysis (lead); Investigation (lead); Methodology (equal); Visualization (lead); Writing – original draft (lead); Writing – review & editing (lead). **Pentti Niiranen:** Data curation (lead); Formal analysis (equal); Investigation (equal); Writing – review & editing (equal). **Oscar Alm:** Conceptualization (equal); Funding acquisition (equal); Supervision (equal); Writing – review & editing (equal). **Jonas Lauridsen:** Conceptualization (equal); Funding acquisition (equal); Supervision (equal); Writing – review & editing (equal). **Tommy Larsson:** Conceptualization (equal); Funding acquisition (equal); Supervision (equal); Writing – review & editing (equal). **Henrik Pedersen:** Conceptualization (lead); Funding acquisition (lead); Project administration (lead); Resources (lead); Supervision (lead); Writing – review & editing (equal).

DATA AVAILABILITY

The data that support the findings of this study are available from the corresponding authors upon reasonable request.

REFERENCES

[1]U. Schleinkofer, C. Czettl, and C. Michotte, "Coating applications for cutting tools," in *Comprehensive Hard Materials*, edited by D. Mari, V. Sarin, L. Miguel, and C. E. Nebel (Elsevier, Oxford, 2014), pp. 453–469.
[2]I. Krajinović *et al.*, Surf. Coat. Technol. **304**, 134 (2016).
[3]H. C. M. Knoops, L. Baggetto, E. Langereis, M. C. M. van de Sanden, J. H. Klootwijk, F. Roozeboom, R. A. H. Niessen, P. H. L. Notten, and W. M. M. Kessels, J. Electrochem. Soc. **155**, G287 (2008).
[4]G. M. Rignanese, J. Phys.: Condens. Matter **17**, R357 (2005).
[5]H. Yamashita, K. Fukui, S. Misawa, and S. Yoshida, J. Appl. Phys. **50**, 896 (1979).
[6]A. T. Collins, E. C. Lightowlers, and P. J. Dean, Phys. Rev. **158**, 833 (1967).
[7]J. Edwards, K. Kawabe, G. Stevens, and R. H. Tredgold, Solid State Commun. **3**, 99 (1965).
[8]G. A. Slack, R. A. Tanzilli, R. O. Pohl, and J. W. Vandersande, J. Phys. Chem. Solids **48**, 641 (1987).
[9]G. Liu, E. Deguns, L. Lecordier, G. Sundaram, and J. Becker, ECS Trans. **41**, 219 (2011).
[10]K. A. Jones, T. P. Chow, M. Wraback, M. Shatalov, Z. Sitar, F. Shahedipour, K. Udwary, and G. S. Tompa, J. Mater. Sci. **50**, 3267 (2015).
[11]N. Afzal, M. Devarajan, and K. Ibrahim, Eur. Phys. J. Appl. Phys. **67**, 10301 (2014).
[12]T. Ishigaki, S. Tatsuoka, K. Sato, K. Yanagisawa, K. Yamaguchi, and S. Nishida, Int. J. Refract. Met. Hard Mater. **71**, 227 (2018).
[13]E. Rauchenwald, M. Lessiak, R. Weissenbacher, S. Schwarz, and R. Haubner, Defect Diff. Forum **405**, 33 (2020).
[14]H. Holleck, J. Vac. Sci. Technol. A **4**, 2661 (1986).
[15]P. H. Mayrhofer, C. Mitterer, L. Hultman, and H. Clemens, Prog. Mater. Sci. **51**, 1032 (2006).
[16]J. Musil, Surf. Coat. Technol. **125**, 322 (2000).
[17]P. H. Mayrhofer, D. Music, and J. M. Schneider, J. Appl. Phys. **100**, 094906 (2006).
[18]N. Schalk, M. Tkadletz, and C. Mitterer, Surf. Coat. Technol. **429**, 127949 (2022).
[19]I. Endler, M. Höhn, M. Herrmann, R. Pitonak, S. Ruppi, M. Schneider, H. van den Berg, and H. Westphal, Surf. Coat. Technol. **203**, 530 (2008).
[20]J. Kohlscheen and C. Bareiss, Coatings **8**, 72 (2018).
[21]M. Jílek, M. Jílek, F. Mendez Martin, P. H. Mayrhofer, and S. Veprek, Thin Solid Films **556**, 361 (2014).
[22]H. Freller and H. Haessler, Surf. Coat. Technol. **36**, 219 (1988).
[23]Y. Y. Chang and D. Y. Wang, Surf. Coat. Technol. **201**, 6699 (2007).
[24]J. P. Endle, Y. M. Sun, J. Silverman, N. Nguyen, A. H. Cowley, J. M. White, and J. G. Ekerdt, Thin Solid Films **385**, 66 (2001).
[25]S. Gilles, N. Bourhila, S. Ikeda, C. Bernard, and R. Madar, Surf. Coat. Technol. **94–95**, 285 (1997).
[26]C. W. Kim and K. H. Kim, Thin Solid Films **307**, 113 (1997).
[27]A. J. M. Mackus, J. R. Schneider, C. Macisaac, J. G. Baker, and S. F. Bent, Chem. Mater. **31**, 1142 (2019).
[28]C.-W. Hsu, I. Martinovic, R. Magnusson, B. Bakhit, J. Palisaitis, P. O. Å. Persson, P. Rouf, and H. Pedersen, J. Vac. Sci. Technol. A **40**, 060402 (2022).
[29]Plasma & Materials Processing group at Eindhoven University of Technology, "Atomic limits ALD Database," Atomic Limits (2021).
[30]J. Xiang *et al.*, Solid-State Electron. **122**, 64 (2016).
[31]E. Y. Yun, W. J. Lee, Q. M. Wang, and S. H. Kwon, J. Mater. Sci. Technol. **33**, 295 (2017).
[32]M. Juppo, P. Aløn, M. Ritala, and M. Leskelä, Chem. Vap. Deposition **7**, 211 (2001).
[33]K. H. Kim and S. H. Lee, Thin Solid Films **283**, 165 (1996).
[34]J. T. Scheper, K. W. Mesthrige, J. W. Proscia, G. Y. Liu, and C. H. Winter, Chem. Mater. **11**, 3490 (1999).
[35]P. Rouf, J. Palisaitis, B. Bakhit, N. J. O. Brien, and H. Pedersen, J. Mater. Chem. C **2**, 13077 (2021).
[36]Y. M. Sun, J. P. Endle, J. G. Ekerdt, N. M. Russell, M. D. Healy, and J. M. White, Mater. Sci. Semicond. Process. **2**, 253 (1999).
[37]C. H. Winter, P. J. McKarns, and J. T. Scheper, MRS Proc. **495**, 95 (1997).
[38]P. Mpofu, H. Hafdi, J. Lauridsen, O. Alm, T. Larsson, and H. Pedersen, Mater. Adv. **5**, 9259 (2024).
[39]F. Jose, R. Ramaseshan, S. Dash, S. Bera, A. K. Tyagi, and B. Raj, J. Phys. D: Appl. Phys. **43**, 075304 (2010).
[40]J. A. Taylor and J. W. Rabalais, J. Chem. Phys. **75**, 1735 (1981).
[41]D. G. Georgiev, L. W. Rosenberger, Y. V. Danylyuk, R. J. Baird, G. Newaz, G. Shreve, and G. Auner, Appl. Surf. Sci. **249**, 45 (2005).
[42]H. M. Liao, R. N. S. Sodhi, and T. W. Coyle, J. Vac. Sci. Technol. A **11**, 2681 (1993).
[43]G. R. Panghulan, M. R. Vasquez, Y. D. Edañol, N. Chanlek, and L. M. Payawan, J. Vac. Sci. Technol. B **38**, 062203 (2020).
[44]N. R. Mucha, J. Som, J. Choi, S. Shaji, R. K. Gupta, H. M. Meyer, C. L. Cramer, A. M. Elliott, and D. Kumar, ACS Appl. Energy Mater. **3**, 8366 (2020).
[45]G. Hasegawa, A. Kitada, S. Kawasaki, K. Kanamori, K. Nakanishi, Y. Kobayashi, H. Kageyama, and T. Abe, J. Electrochem. Soc. **162**, A77 (2015).
[46]S. Jiang, B. Yi, H. Zhang, W. Song, Y. Bai, H. Yu, and Z. Shao, ChemElectroChem **3**, 734 (2016).
[47]N. R. Mucha, J. Som, S. Shaji, S. Fialkova, P. R. Apte, B. Balasubramanian, J. E. Shield, M. Anderson, and D. Kumar, J. Mater. Sci. **55**, 5123 (2020).
[48]J. Y. Kim, H. K. Kim, Y. Kim, Y. Do Kim, W. M. Kim, and H. Jeon, J. Korean Phys. Soc. **40**, 176 (2002).
[49]D. M. Hoffman, S. P. Rangarajan, S. D. Athavale, D. J. Economou, J.-R. Liu, Z. Zheng, and W.-K. Chu, J. Vac. Sci. Technol. A **14**, 306 (1996).
[50]D. M. Hoffman, U. Riaz, and Roy G. Gordon, J. Mater. Res. **7**, 1679 (1992).
[51]Y. Takahashi, K. Mutoh, S. Motojima, and K. Sugiyama, J. Mater. Sci. **16**, 1217 (1981).
[52]A. Berry, R. Mowery, N. H. Turner, L. Seitzman, D. Dunn, and H. Ladouceur, Thin Solid Films **323**, 10 (1998).
[53]K. C. Park, K. B. Kim, I. J. M. M. Raaijmakers, and K. Ngan, J. Appl. Phys. **80**, 5674 (1996).
[54]E. O. Travis and R. W. Fiordalice, Thin Solid Films **236**, 325 (1993).
[55]S. Anderbouhr, S. Gilles, E. Blanquet, C. Bernard, and R. Madar, Chem. Vap. Deposition **5**, 109 (1999).
[56]R. G. Gordon, D. M. Hoffman, and U. Riaz, J. Mater. Res. **6**, 5 (1991).
[57]J. Lee, J. Kim, and H. Shin, Thin Solid Films **320**, 15 (1998).
[58]M. Zhou, Y. Makino, M. Nose, and K. Nogi, Thin Solid Films **339**, 203 (1999).
[59]J. Musschoot, Q. Xie, D. Deduytsche, S. Van den Berghe, R. L. Van Meirhaeghe, and C. Detavernier, Microelectron. Eng. **86**, 72 (2009).
[60]D. M. Hoffman, Polyhedron **13**, 1169 (1994).
[61]K. Sen, T. Banu, T. Debnath, D. Ghosh, and A. K. Das, Dalton Trans. **43**, 8877 (2014).
[62]NIST, "NIST-JANAF thermochemical tables," NIST Stand. Ref. Database 13 (2013).
[63]H. Hamdi and H. R. Abedi, J. Mater. Res. Technol. **30**, 4424 (2024).
[64]Y. J. Lee and S. W. Kang, Electrochem. Solid-State Lett. **6**, C70 (2003).
[65]J. H. Kim, J. Y. Kim, and S. W. Kang, J. Appl. Phys. **97**, 093505 (2005).
[66]D. R. Lide, *CRC Handbook of Chemistry and Physics* (CRC, Boca Raton, 2005). http://www.hbcpnetbase.com.
[67]N. N. Greenwood and A. Earnshaw, *Chemistry of the Elements*, 2nd ed. (Reed Educational and Professional Publishing Ltd, Oxford, 1997).
[68]A. Forslund and A. Ruban, Comput. Mater. Sci. **183**, 109813 (2020).
[69]E. Härkönen *et al.*, J. Electrochem. Soc. **158**, C369 (2011).